JMEPEG (1997) 6:757-765

Simulation of Vertical-Horizontal Rolling Process during Width Reduction by Full Three-Dimensional Rigid-Plastic Finite Element Method

S. Xiong, X. Liu, G. Wang, and W. Zhang

Vertical-horizontal (V-H) rolling is an important process during width reduction in the roughing stand of hot strip mill. A simulation of steady-state V-H rolling was carried out by the full three-dimensional rigid-plastic finite element method (3D RPFEM). To consider the shear work rate and cope with a singular point, an extremely thin array of elements was attached before the entry of the roll. The slab shape, the spread, the separating force, and the rolling torque calculated were in good agreement with the experimental values.

Keywords extremely thin element, finite element method, vertical-horizontal rolling

1. Introduction

In order to expand a synchronized operation between the continuous slab casting and hot rolling processes, heavy width reduction is widely obtained by either rolling or pressing in roughing trains of hot strip mill. The V-H rolling process is still important (Ref 1, 2). Some simulations by FEM have been done by K. Mori (Ref 3), Huisman and Huetink (Ref 4), and C. David et al. (Ref 5) on slab edging with flat roll, and by Nikado et al. (Ref 6) on the whole V-H rolling process. But there have been problems with precision due to an overly simplified 3D model and other assumptions.

In this study, an analysis of the V-H rolling process was carried out by full 3D RPFEM, considering the effect of width reduction, initial slab width, and edger diameter. The influence of the velocity of the flat edger roll on the slab shapes edged, the diameter of the horizontal roll on additional bar width spread due to bulging, and the velocity of the horizontal roll on the bar width spread after subsequent horizontal rolling are studied.

2. Theoretical Analysis

2.1 *Basic Equations*

According to RP FEM, if no tractions are applied to the entry and exit surfaces of the workpiece, the function φ to be minimized is given by (Ref 7):

$$\Phi = \iiint_V \bar{\sigma}\,\dot{\bar{\varepsilon}}\,dV + \int_{S_j} \tau_s \Delta v_j dS + \int_{S_\tau} \tau_f \Delta v_f dS \qquad \text{(Eq 1)}$$

where $\bar{\sigma}$ is the equivalent stress, $\dot{\bar{\varepsilon}}$ is the equivalent strain rate, Δv_j is the velocity discontinuity across the velocity discontinuity surface S_j within the volume V, and Δv_f is the relative slipping velocity on the interface of roll and workpiece where friction τ_f is applied. S. Kobayashi friction (Ref 8) is assumed:

$$\tau_f = m_k \tau_s \left(\frac{2}{\pi} \tan^{-1} \left\{ \frac{\Delta V_f}{V_a} \right\} \right) \qquad \text{(Eq 2)}$$

where m_k is the friction factor, τ_s is the shear yield stress, $\tau_s = \frac{\sigma_s}{\sqrt{3}}$, and V_a is a small positive constant. In this paper, $m_k = 0.65$.

The relative velocity Δv_f of the slab-roll is approximated by:

$$\Delta v_f = \sqrt{(u \sec \beta - V_R)^2 + v^2 + e_1^2} \qquad \text{(Eq 3)}$$

where u and v are the velocity components in directions x and y, respectively, β is the angular position of the node, V_R is the roll velocity, and e_1 is a small positive constant to prevent distortion during calculation (Ref 9).

When the function Φ is minimized according to the Newton-Rophson method (Ref 9), the stress tensor can be found (Ref 9):

$$\sigma_{ij} = \frac{\bar{\sigma}}{\dot{\bar{\varepsilon}}} \left(\frac{2}{3} \dot{\varepsilon}_{ij} + \delta_{ij} (g - \frac{2}{9}) \dot{\varepsilon}_v \right) \qquad \text{(Eq 4)}$$

where $\dot{\varepsilon}_{ij}$ is the strain rate tensor, δ_{ij} is the Kronecker delta, g is a small positive constant, and $\dot{\varepsilon}_v = \dot{\varepsilon}_x + \dot{\varepsilon}_y + \dot{\varepsilon}_z$.

2.2 *FEM Mesh*

The isoparametric hexahedron element with eight Gauss points was used throughout in the slab, even for the corner at the entrance. To cope with this singular point, only an extremely thin array of elements was attached before the corner of the roll entry (thickness of these elements $dx_1 << dl$) (Ref 7), as shown in Fig. 1. Moreover, there was a noncontact region during subsequent horizontal rolling, FE mesh as given in Fig. 2. A simple linear interpolation was carried out to determine the true point of roll-slab surface. Interpolation function N_i and partial differential etc. in the elements containing these points were changed as a result, so the area of friction region and the friction energy were obtained precisely.

S. Xiong, X. Liu, G. Wang, and **W. Zhang,** State Key Laboratory of Rolling Technology and Automation of Tandem Rolling, Northeastern University, Shenyang, 110006, P.R. China.

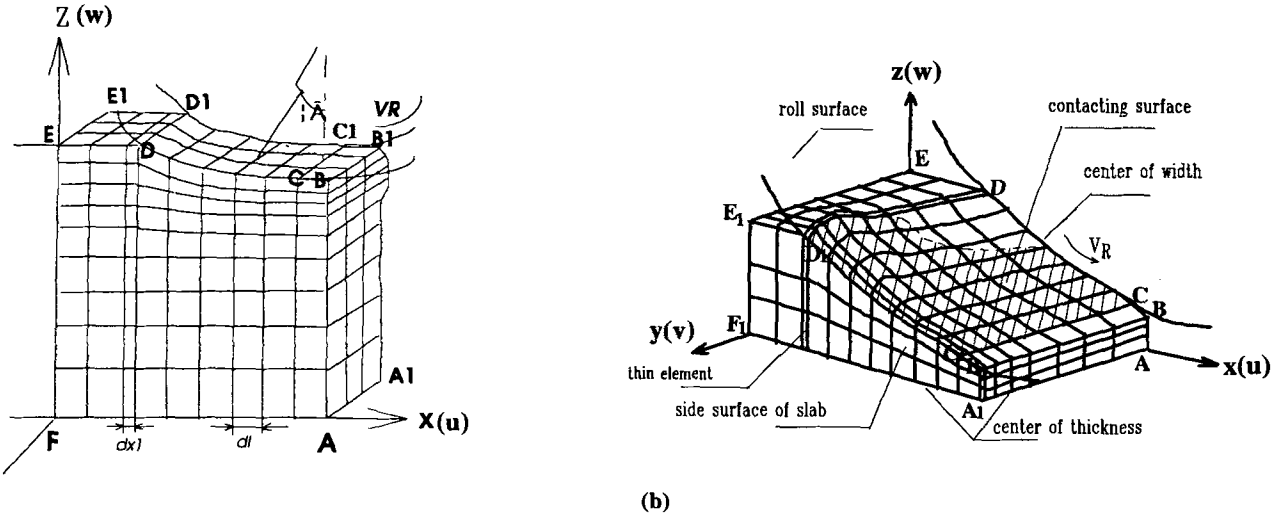

Fig. 1 The FE meshes in (a) slab edging, (b) subsequent horizontal rolling

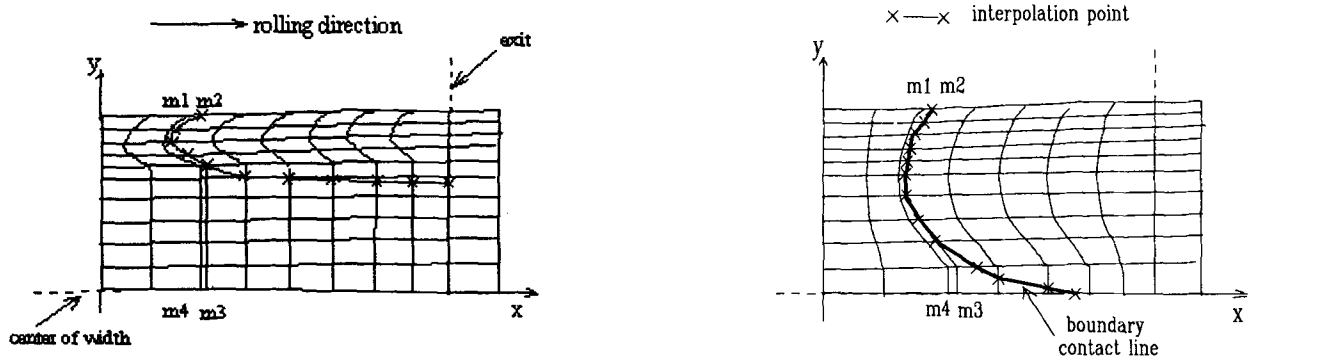

Fig. 2 Treatment of the contact region during subsequent horizontal rolling. (a) $\Delta H = 0$. (b) $\Delta H > 0$

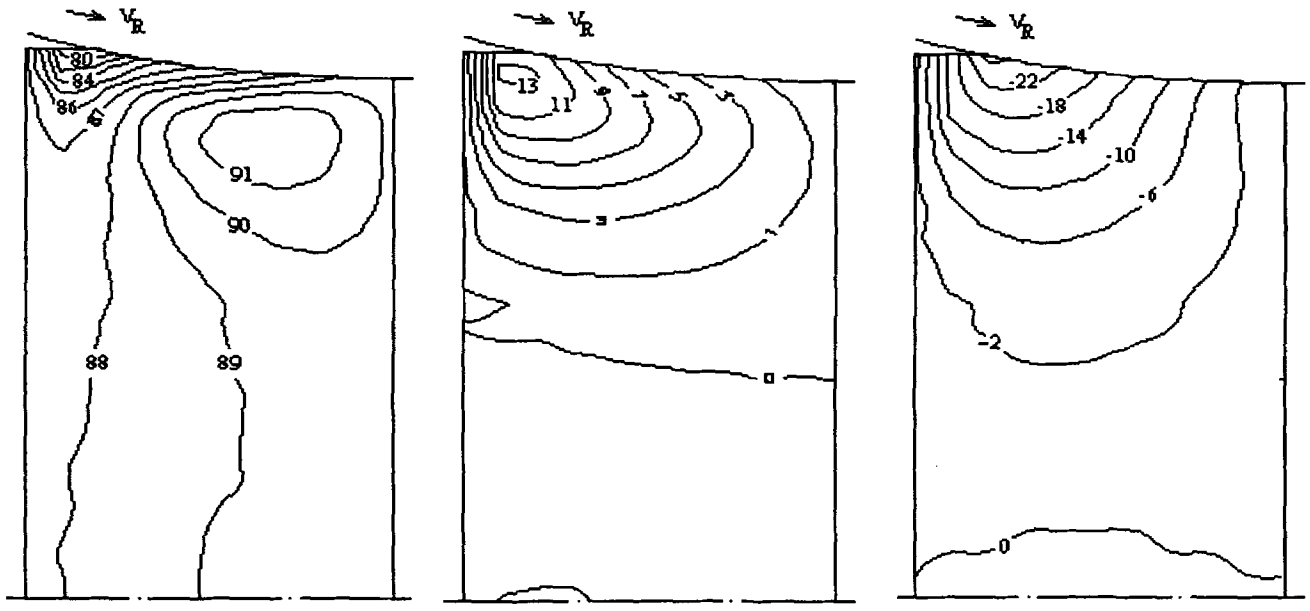

Fig. 3 Velocity components in section A1B1E1F1 (H_0 = 15.4 mm, B_0 = 108 mm, ΔE = 6.1 mm)

2.3 *Velocity Boundary Conditions*

Because the deformation was symmetrical about both the y-x and z-x planes, we took its 1/4 part as the study object, as shown in Fig. 1. For slab edging, there were 2 to 3 rows of elements in the thickness direction y, 12 rows in the width direction z, and 9 to 12 arrays in the rolling direction x, in which three arrays were for the entry region (including one array of extremely thin element) and one array was for the exit region. The velocity boundary conditions were:

- AA1B1B: $u = u_0$ (unknown), $v = w = 0$
- EFF1E1: $u = u_1$ (unknown), $v = w = 0$
- CDD1C1: $w/u = -\text{tg}\beta$
- BCC1B1: $w = 0$
- FF1A1A: $w = 0$
- EFAB: $v = 0$

where u, v, and w are the velocity components in directions x, y, and z, respectively.

For subsequent horizontal rolling, the velocity boundary conditions were:

- AA1B1B: $u = u_0$ (unknown), $v = w = 0$
- EFF1E1: $u = u_1$ (unknown), $v = w = 0$
- Contact region: $w/u = -\text{tg}\beta$
- BCC1B1: $w = 0$
- FF1A1A: $w = 0$
- EFAB: $v = 0$

where u, v, and w are the velocity components in directions x, y, and z, respectively.

3. Results

3.1 *Experimental and Calculating Conditions*

A model material, lead, with a scale of 1:10 was used to simulate the width reduction process of Benxi Hot Strip Mill in State Key Laboratory of Rolling Technology and Automation of Tandem Rolling, P.R. China.

Two conditions were studied:

- The effect of edger diameter, D_e. Slab: $H_0 = 15.4$ mm, $B_0 = 108$ mm. $D_e = 62$ to 105 mm. Width reduction: $\Delta E = 2$ to 6.5 mm.

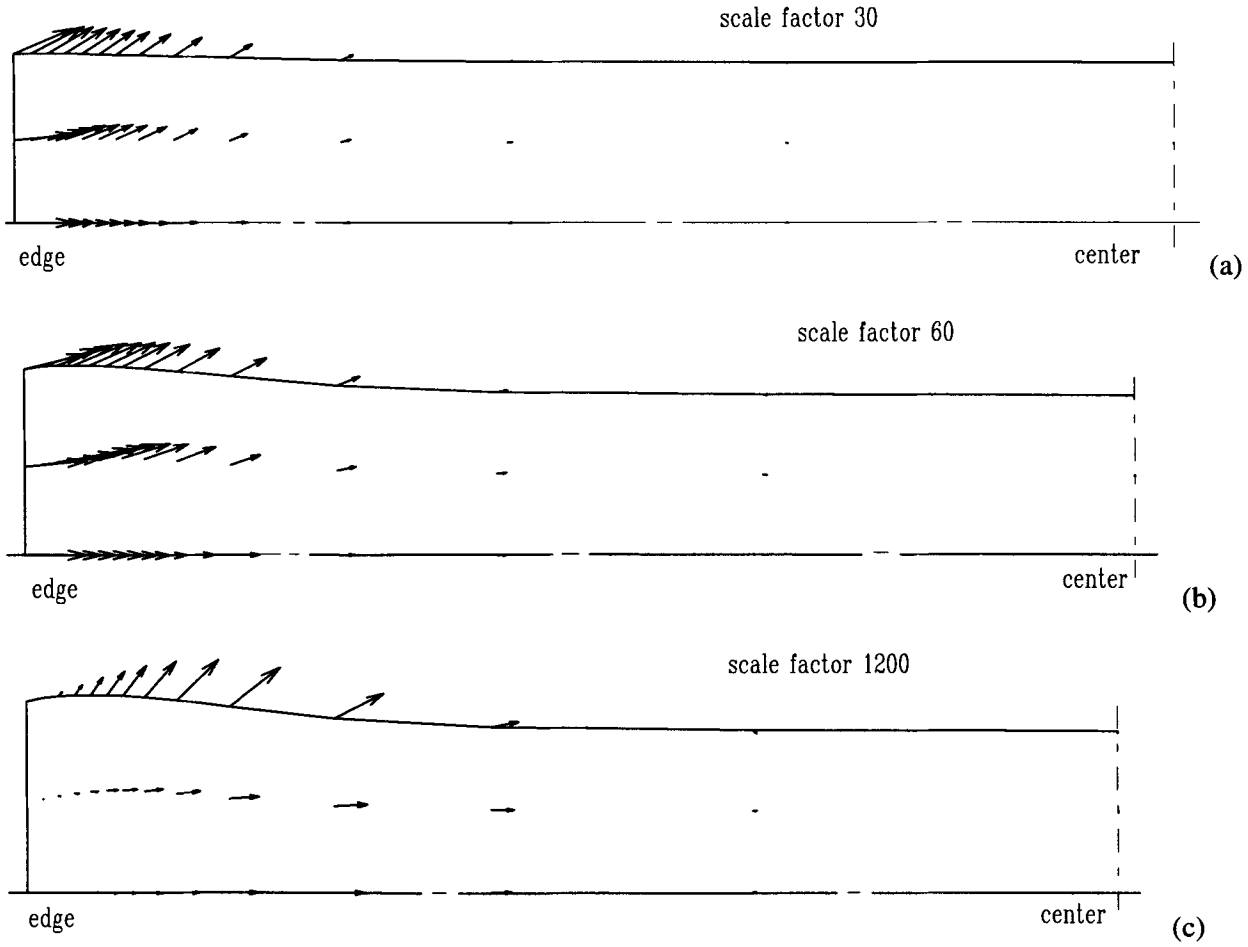

Fig. 4 Velocities in three cross sections of the slab during edging ($H_0 = 15.4$ mm, $B_0 = 108$ mm, $\Delta E = 6.1$ mm). (a) At entrance. (b) Halfway across the contact zone. (c) At the roll-gap exit

- The effect of slab width, B_0. Slab: $H_0 = 20$ mm. $B_0 = 75$ mm, 100 mm. $D_e = 105$ mm. Width reduction: $\Delta E = 2$ to 10 mm.

The other working conditions were: velocity of edger, 19 rpm; horizontal roll diameter, D_H, 130 mm; velocity of horizontal roll, 27.5 rpm; and thickness reduction, ΔH, 0 to 3 mm.

The roll, made of common carbon steel, was supposed to be a rigid model. The flow stress of work-hardening lead was (Ref 10):

$$\sigma = 13.24 \exp\left(\frac{370}{273 + t}\right)\dot{\varepsilon}^{0.07}\varepsilon^{0.33} \text{ (MPa)} \qquad \text{(Eq 5)}$$

where t is temperature in degrees Celsius, taken as 25 °C here.

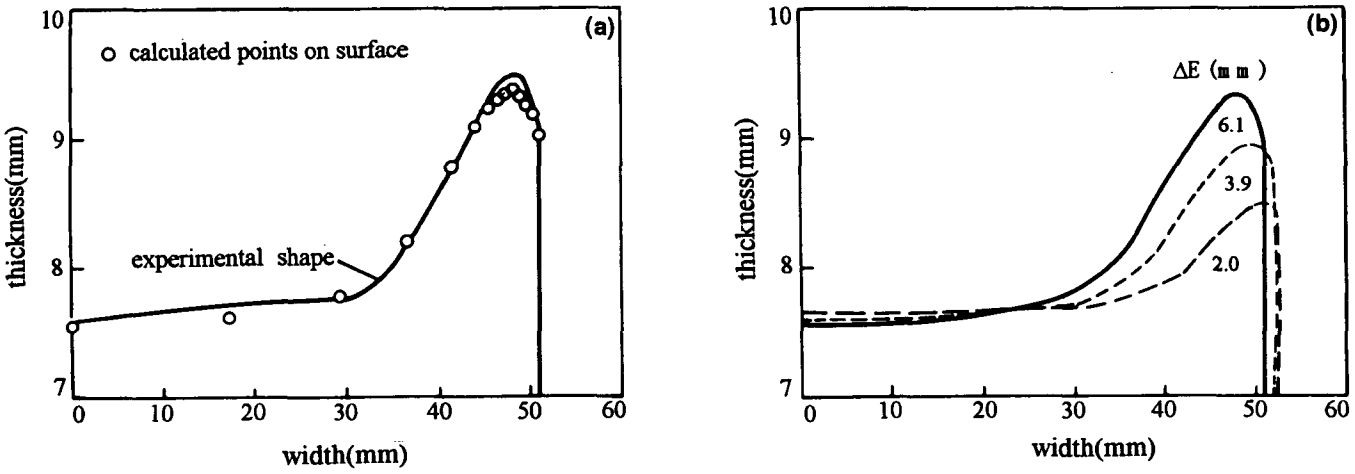

Fig. 5 (a) One-quarter sectional shape calculated with experimental one. $H_0 = 15.4$ mm, $B_0 = 108$ mm, $\Delta E = 6.1$ mm. (b) One-quarter sectional shape calculated in various width reductions. $H_0 = 15.4$ mm, $B_0 = 108$ mm

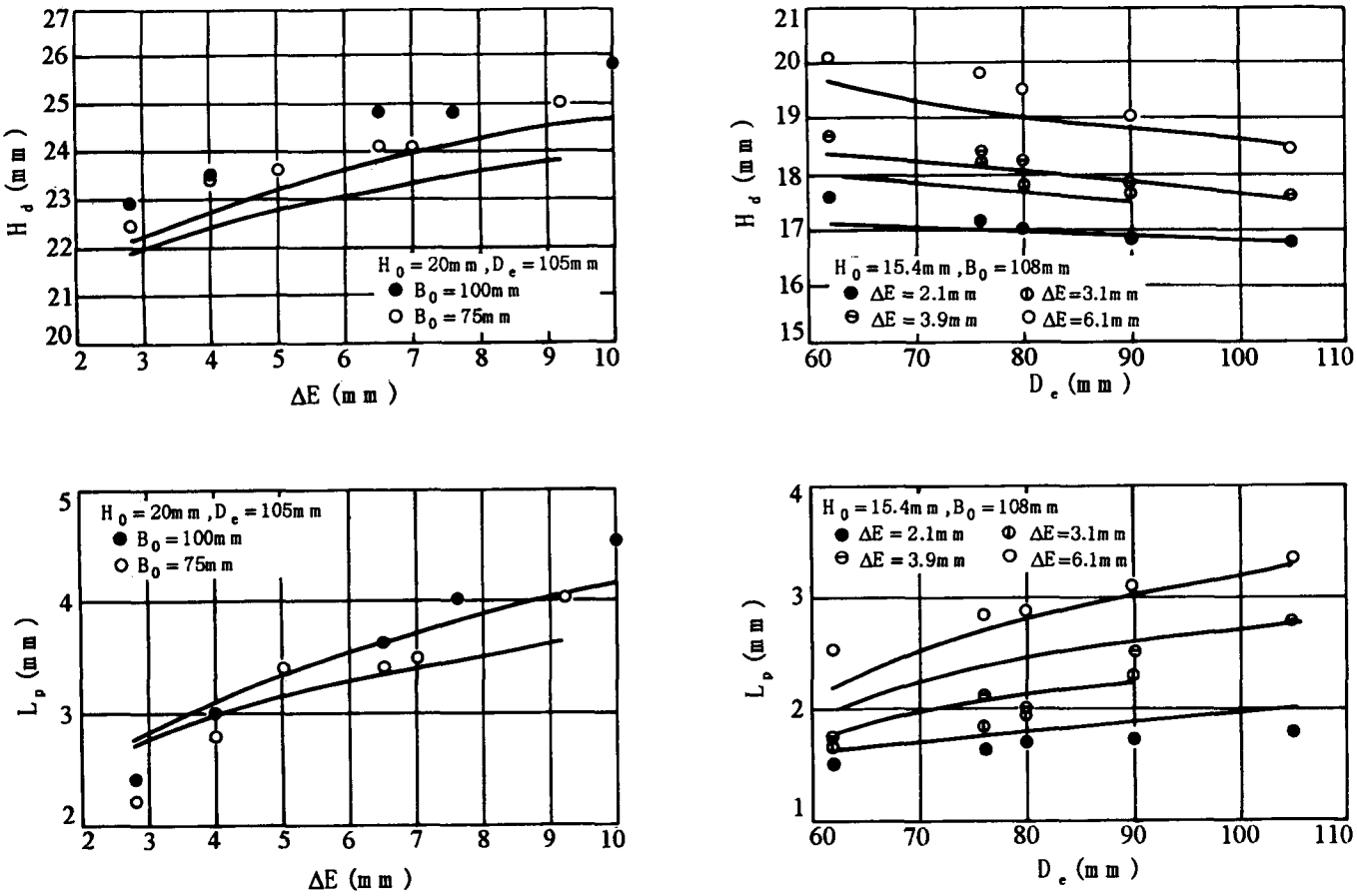

Fig. 6 The effect of ΔE on H_d and L_p

3.2 *Calculated Results*

3.2.1 Slab Edging

The velocity field in the rolling direction (x), the thickness direction (y), and the width direction (z) in the edge transverse-section of the slab (shown in Fig. 1a) are drawn in Fig. 3. The velocity components v and w show the maximum values near the slab edge in the roll entry, and they decrease from the slab edge toward the slab center, while u shows the opposite results.

The distribution of the velocities in the y and z directions, in three typical cross sections of the slab, are shown in Fig. 4. From Fig. 4(a) and (b), it is obvious that the slab material near the center does not move significantly in either of the two directions, at entrance or halfway along the contact arc. Therefore, a "dogbone" shape is formed near the slab edge.

Figures 5(a) and (b) are examples of the sectional shape of slab calculated after edging. They show that as the width reduction increases, the thickness increases in the vicinity of the con-

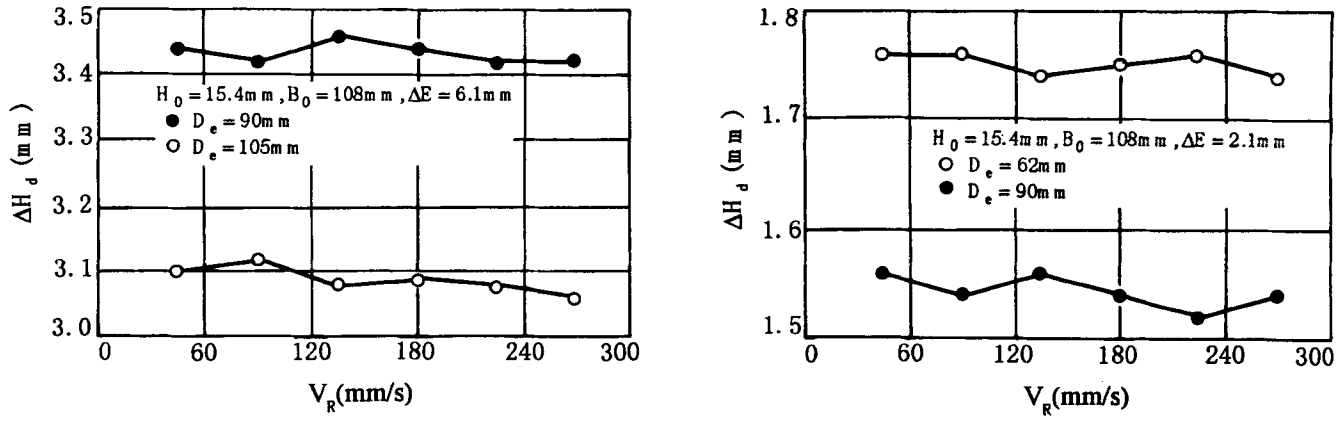

Fig. 7 Influence of rolling velocity on calculated ΔH_d ($= H_d - H_0$) (15.4 × 108 mm)

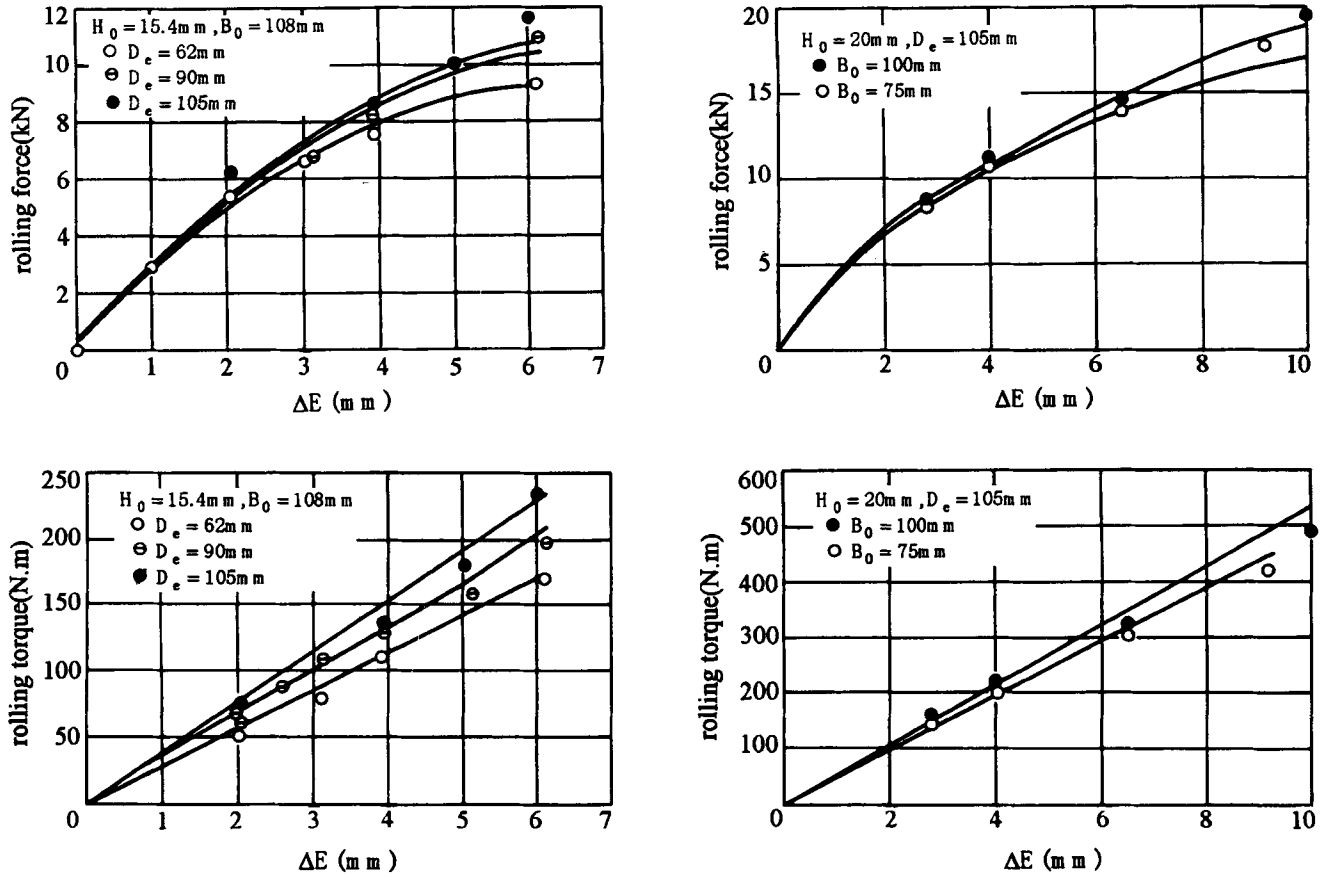

Fig. 8 Comparison of calculated separation force and rolling torque with experimental values

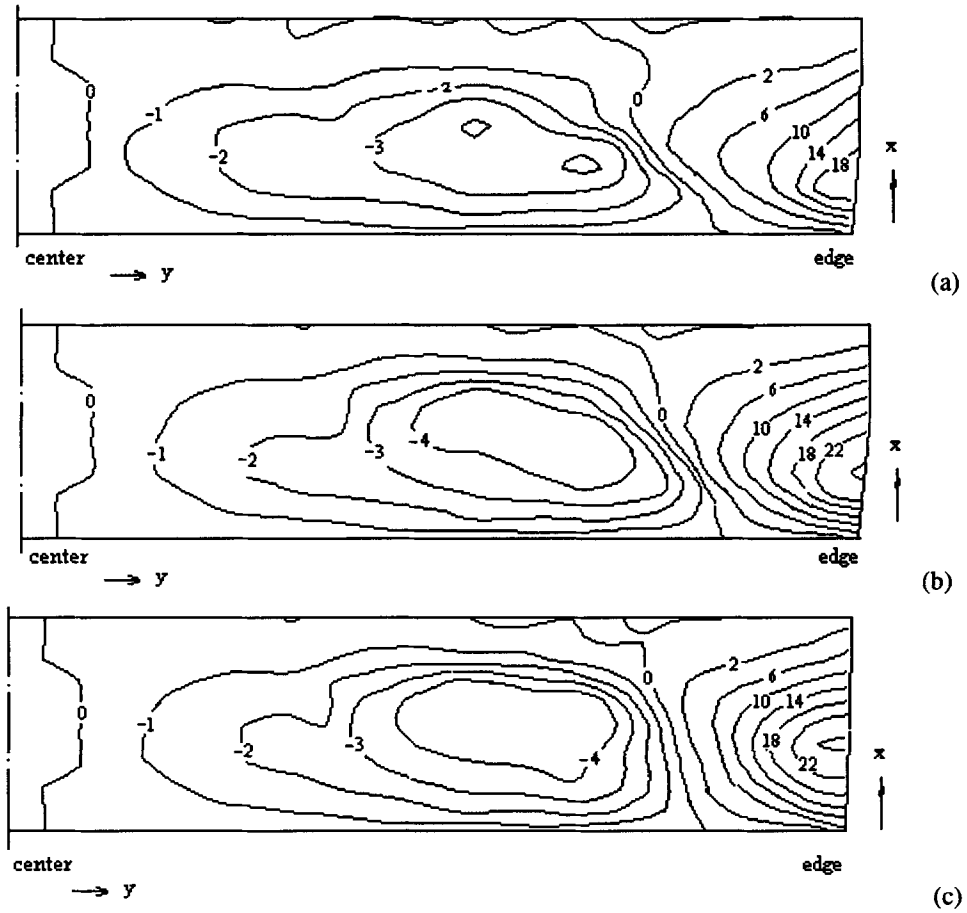

Fig. 9 Velocity component v (in width direction y) in three horizontal sections during rolling. (a) At surface. (b) Quarter thickness (halfway in Fig. 1b). (c) Middle in thickness direction z. Slab: H_0 = 15.4 mm, B_0 = 108 mm, ΔE = 6.1 mm, ΔH = 2 mm

tact, while the thickness in the center of the width hardly changes.

Dogbone thickness H_d and the peak position L_p are usually used as important shape parameters to characterize the shape of slab edge (Ref 1, 2). The calculations are given in Fig. 6. It shows that H_d and L_p increase with width reduction ΔE and initial slab width B_0, and L_p increases with edger diameter D_e while H_d decreases. The results are in good agreement with the experimental values.

The FE results show that there are only small effects of the velocity of the roll V_R on the shape parameters. Figure 7 is an example of H_d versus V_R. This explains why V_R is neglected in empirical models of shape parameters (Ref 1, 2).

The influence of ΔE on the rolling force P and torque M is shown in Fig. 8, which shows that P and M increase with ΔE and D_e. The contact length and the velocity of the roll increase as D_e, and the velocity of rotation is a constant. Moreover, P and M increase with B_0.

3.2.2 Horizontal Rolling

As an example, the distribution of velocity component v (in the width direction y) in three horizontal sections is presented in Fig. 9. It shows that material in the left of the dogbone shrinks toward the width center slightly, while material in the dogbone tends to spread, which differs from common horizontal rolling. Moreover, there is no obvious difference among these sections, only a greater gradient of v in the width direction y in Fig. 9(b) and (c) than in (a). The maximum of v occurs near the slab edge.

When edging is followed by a reduction in thickness, the bar width spread after thickness reduction ΔB will consist of two parts (Ref 2):

$$\Delta B = \Delta B_b + \Delta B_s \qquad \text{(Eq 6)}$$

where ΔB_b is bar width spread due to bulging after reduction in thickness and ΔB_s is bar width spread after reduction in thickness, excluding the width increase caused by spread of bulges.

Figure 10 compares the calculated values for bar width spread with experimental values. Bar width spread increases with increases in width reduction and thickness reduction, and it decreases with edger roll diameter. Moreover, FE simulations show that there is little influence of the work roll diameter used in thickness reduction on ΔB_b, which is similar to the experimental results obtained by Kokado et al. (Ref 11). The influence of velocity of horizontal roll on ΔB is shown in Fig. 11.

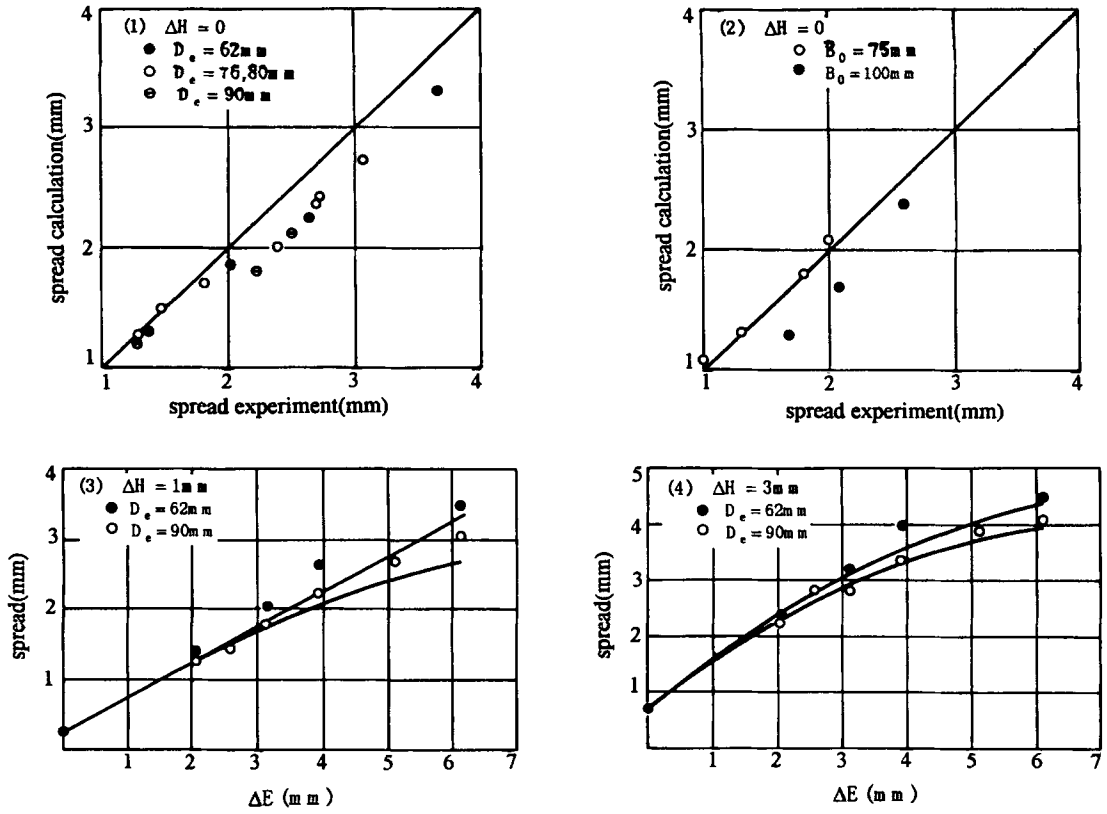

Fig. 10 Comparison of calculated width spread with experimental values

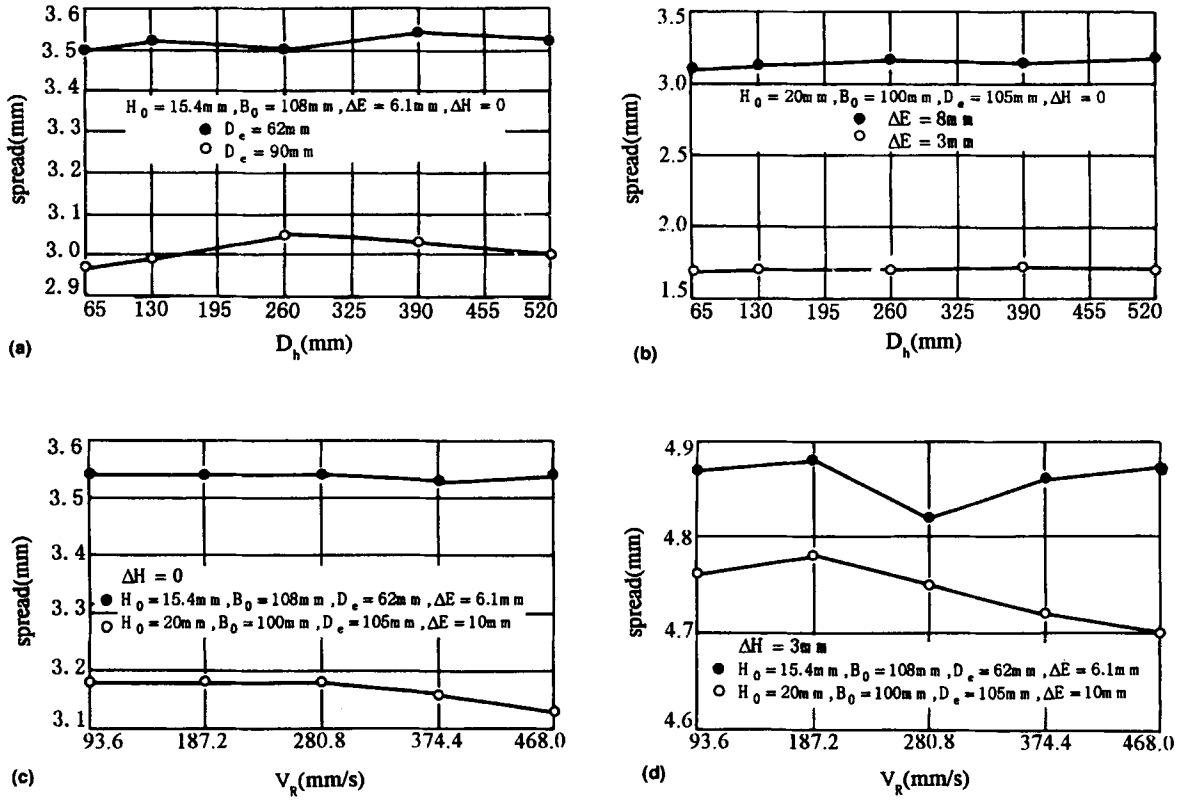

Fig. 11 (a) and (b) Calculated results of the effect of horizontal roll diameter on width spread. (c) and (d) Calculated results of the effect of horizontal roll velocity on width spread

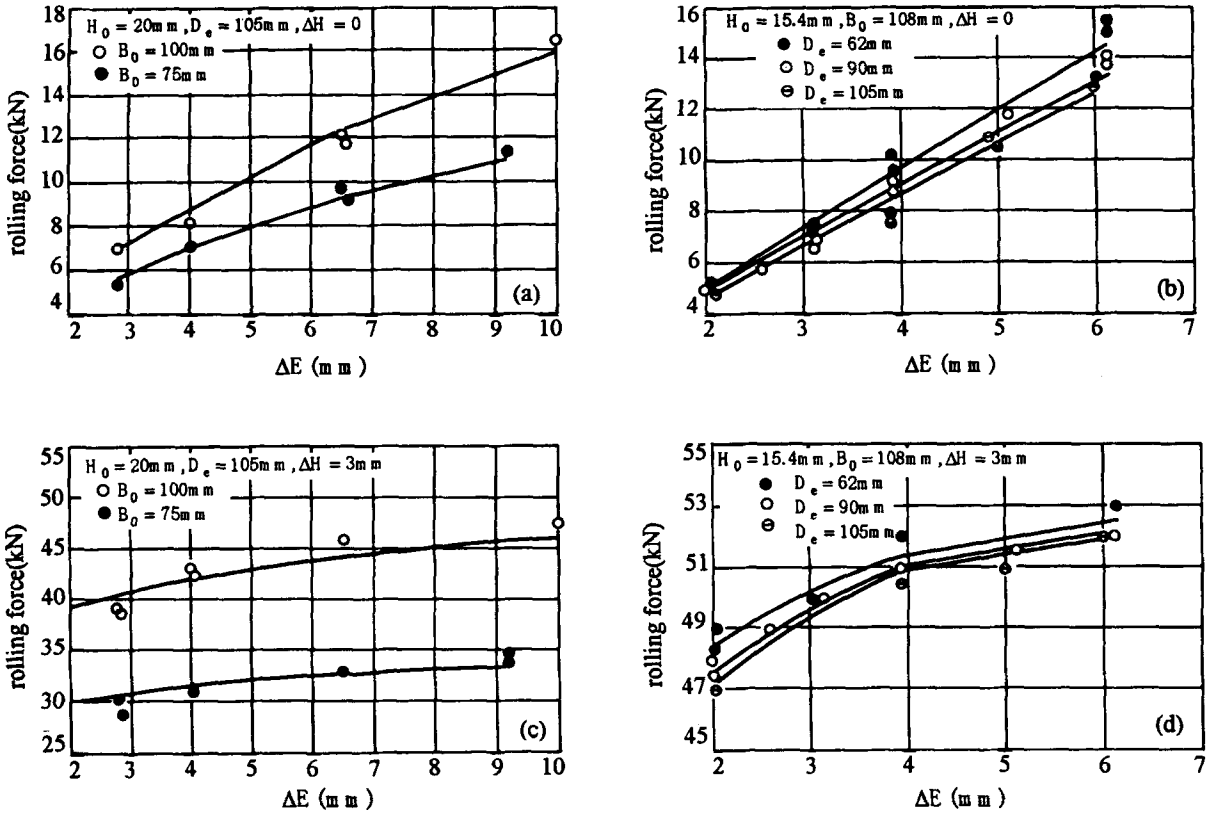

Fig. 12 Comparison of calculated rolling force during horizontal rolling with experimental values

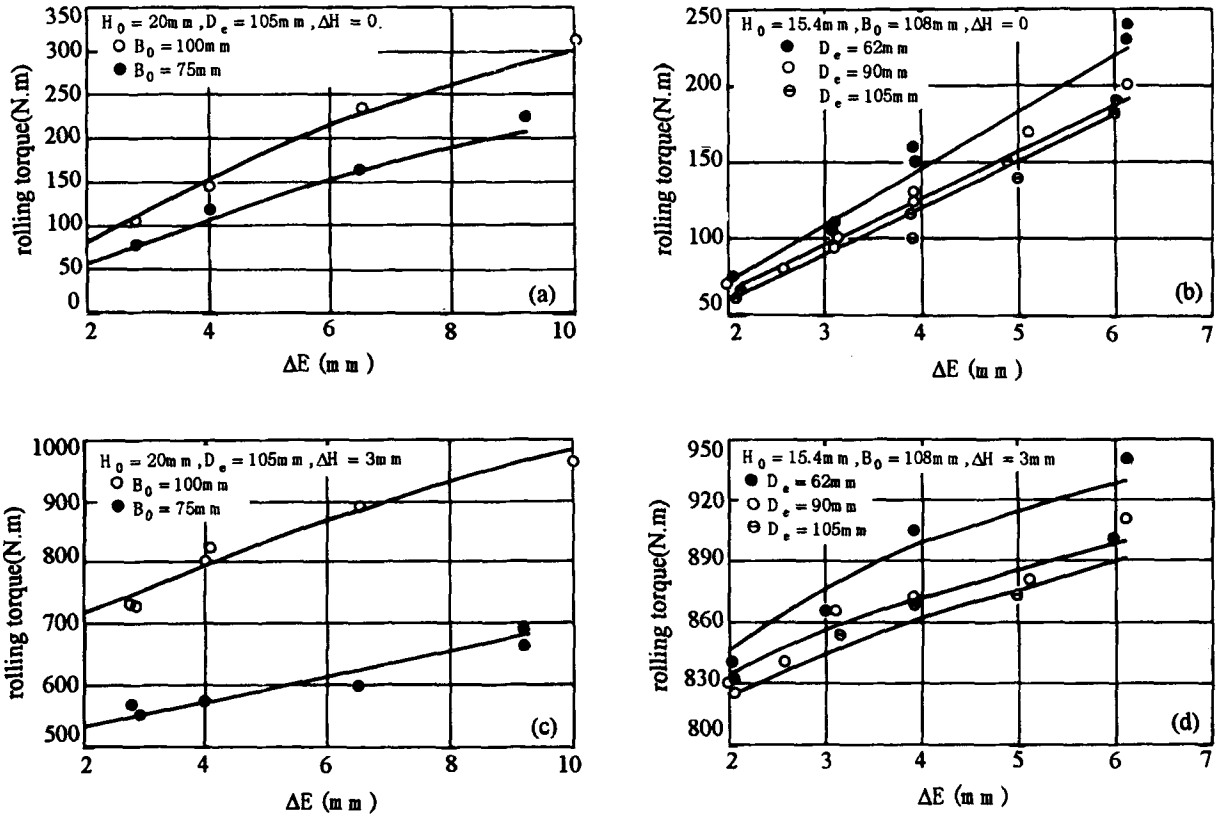

Fig. 13 Comparison of calculated rolling torque during horizontal rolling with experimental values

The horizontal rolling force P_H and rolling torque M_H increase with initial slab width B_0 and width reduction ΔE, and they decrease with the edging roll diameter. The comparison with experimental results shows a good agreement, as shown in Fig. 12 and 13.

4. Conclusions

Full 3D RPFEM has been applied to solve the V-H rolling process for lead. To consider the shear energy and cope with a singular point, an extremely thin array of element was attached before the entry of the roll. Comparisons with experimental results show that this method can be used to simulate the process accurately.

FE simulations show several important results:

- There are relatively great influences of width reduction, initial slab width, and edger diameter on the slab edged, whereas the effect of the edging velocity need not be taken into account.
- There are obvious effects of width reduction, initial slab width, and edger diameter on the bar width spread after subsequent thickness reduction. However, the effect of the diameter of the work roll on additional bar width spread due to bulging, and the effect of the rolling velocity on the bar width spread, can be neglected.

References

1. M. Okado, T. Arizumi, Y. Noma, K. Yabuuchi, and Y. Yamazaki, Width Behavior of Head and Tail of Slabs at Edging Rolling in Hot Strip Mills, *J. Iron and Steel Inst. Jpn.*, Vol 67, 1981, p 2516-2525
2. V.B. Ginzburg, *Steel Rolling Technology: Theory and Practice,* Marcel Dekker, New York, 1989
3. K. Mori and K. Osakada, Simulation of Three-Dimensional Rolling by the Rigid-Plastic Finite Element Method, *Proc. Int. Conf. Numerical Methods in Industrial Forming Processes,* Pineridge Press, Swansea, 1982, p 747-756
4. H.J. Huisman and J. Huetink, A Combined Eulerian-Langrangian Three-Dimensional Finite-Element Analysis of Edge-Rolling, *J. Mech. Work. Technol.*, Vol 21, 1985, p 333-353
5. C. David, C. Bertrand, J.L. Chenot, and P. Buessler, A Transient 3D FEM Analysis of Hot Rolling of Thick Slabs, *Conf. Proc. Numiform '86,* K. Mattiasson et al., Ed., Balkema, 1986, p 219-224
6. H. Nikaido, T. Naoi, K. Shibata, T. Kondo, K. Osaka, and K. Mori, Numerical Simulation of Width Spread of "Dog-Bone" Slab in Non-Steady Horizontal Rolling, *J. Jpn. Soc. Technol. Plast.*, Vol 25 (No. 277), 1984, p 129-135
7. X. Shangwu, L. Xianghua, W. Guodong, and Z. Qiang, Simulation of Slab Edging by Full 3D R.P. FEM, *Proc. Int. Conf. MSMM '96,* Metallurgical Industry Press, 1996, p 589-592
8. S. Kobayashi et al., *Metal Forming and the Finite Element Method,* Oxford University Press, 1989
9. L. Xianghua, "Experiments and Analysis by Rigid-Plastic FEM on the Process of Rolling H-Beam with Tensions on a Universal Mill," Ph.D. dissertation, Northeastern University, 1985 (in Chinese)
10. K. Nakajima, H. Kamo, S. Yanagimoto, K. Watanabe, Y. Tonoya, and N. Miki, New Light on Theory of Section Rolling, *Seitetus Kenkyu,* No. 275, 1972, p 42-46
11. J. Kokado, N. Hatta, and H. Takuda, Influences of Roll Diameter and Slab Width on Rolling Characteristics in Width Reduction of Slab, *J. Jpn. Soc. Technol. Plast.*, Vol 24, 1983, p 1150-1165